

DETECTING HIGH REDSHIFT EVOLVED GALAXIES AS THE HOSTS OF OPTICALLY FAINT HARD X-RAY SOURCES¹

L. L. COWIE,^{2,3} A. J. BARGER,^{2,3,4,5} M. W. BAUTZ,⁶ P. CAPAK,² C. S. CRAWFORD,⁷ A. C. FABIAN,⁷
E. M. HU,^{2,3} F. IWAMURO,⁸ J.-P. KNEIB,⁹ T. MAIHARA,⁸ K. MOTOHARA⁸

Astrophysical Journal Letters in press

ABSTRACT

We combine deep Subaru near-infrared images of the massive lensing clusters A2390 and A370 with Keck optical data to map the spectral energy distributions (SEDs) of *Chandra* X-ray sources lying behind the clusters. The three sources behind A2390 are found to have extremely red colors with SEDs consistent with evolved galaxies at redshifts $z > 1.4$. One source has extremely anomalous colors, which we interpret as evidence for a type Sa SED at a redshift around 2.5. The photometric redshift of another source has been confirmed at $z = 1.467$ from near-infrared spectroscopy using the CISCO spectrograph on Subaru. Mapping of optically faint hard X-ray sources may prove to be an extremely efficient way to locate luminous evolved galaxies at high redshifts.

Subject headings: cosmology: observations — galaxies: distances and redshifts — galaxies: evolution — galaxies: formation — galaxies: active — galaxies: starburst

1. INTRODUCTION

Recent deep surveys with the *Chandra* X-ray Observatory have resolved most of the hard (2 – 7 keV) X-ray background (XRB) into a population of point sources (Mushotzky et al. 2000; Giacconi et al. 2001), about two-thirds of which are optically bright enough to be spectroscopically identified (Barger et al. 2001; Hornschemeier et al. 2001). A substantial fraction of the spectroscopically identified sources lie in the nuclei of luminous bulge-dominated galaxies whose integrated optical spectra often show little sign of the nuclear activity. The remaining third of the hard X-ray sources are optically faint ($I > 23.5$) with $I - K$ colors that are very red. It has been speculated that many of these optically faint sources may simply be higher redshift analogs of the $z < 1.5$ luminous galaxy hosts, since the red SEDs would result in substantial optical fading at higher redshift (Crawford et al. 2000; Barger et al. 2001).

In order to fully understand the origins of the hard XRB and to determine the evolution of the space density of AGN, we need to know the nature and redshift distribution of the optically faint hard X-ray sources. Furthermore, if it can be securely demonstrated that some of the optically faint hard X-ray sources do indeed lie in evolved galaxies at redshifts $z > 1.5$, then the very existence of such systems will be of enormous interest in understanding the timescales for galaxy formation. The combination of hard X-ray and optical data would then provide an extremely efficient technique for locating such sources.

Robust redshifts for evolved galaxies can be obtained from their SEDs. Since much of the signal for such an analysis lies in the relative slope above and below the 4000 Å break, we need good infrared photometry for this purpose.

We have obtained deep near-infrared (NIR) imaging of the cores of two massive lensing clusters observed by *Chandra*, A2390 ($z = 0.23$) and A370 ($z = 0.37$), to map the SEDs of the X-ray sources that lie behind the clusters. The advantage of targeting X-ray fields with foreground ($z = 0.2 - 0.4$) massive cluster lenses is that any source lying behind will be substantially magnified.

The two hard X-ray sources detected behind the A370 cluster by Bautz et al. (2000) are optically bright and have been spectroscopically identified ($z = 1.060$ and $z = 2.8$; Soucail et al. 1999; Barger et al. 1999; Ivison et al. 1998). Their spectra show strong AGN signatures, their morphologies are unusual, and both are strong submillimeter sources (Bautz et al. 2000; Smail, Ivison & Blain 1997). In contrast, the three X-ray sources detected behind the A2390 cluster by Fabian et al. (2000) are all coincident with relatively smooth red galaxies (Fig. 1). Henceforth we refer to these as Sources 1 (CXOUJ215334.0+174242), 2 (CXOUJ215333.8+174116), and 3 (CXOUJ215333.2+174211) (see Fig. 1). These sources are not known submillimeter sources and do not have optical spectroscopic redshifts (Crawford et al. 2000; Fabian et al. 2000). While the faintest of these sources (Source 2) is only detected in the soft band of this still relatively shallow X-ray image, the three sources appear to be representative of the optically faint hard X-ray source

¹Based in part on data collected at the Subaru Telescope, which is operated by the National Astronomical Society of Japan

²Institute for Astronomy, University of Hawaii, 2680 Woodlawn Drive, Honolulu, Hawaii 96822

³Visiting Astronomer, W. M. Keck Observatory, jointly operated by the California Institute of Technology, the University of California, and the National Aeronautics and Space Administration

⁴Hubble Fellow and Chandra Fellow at Large

⁵Department of Astronomy, University of Wisconsin, 475 North Charter Street, Madison, WI 53706

⁶Center for Space Research, 70 Vassar Street, Building 37, Massachusetts Institute of Technology, Cambridge, MA 02139

⁷Institute of Astronomy, Madingley Road, Cambridge CB3 0HA, U.K.

⁸Department of Physics, Faculty of Science, Kyoto University, Sakyo-ku, Kyoto 606-8502, Japan

⁹Observatoire Midi-Pyrénées, 14 Avenue E. Belin, 31400 Toulouse, France

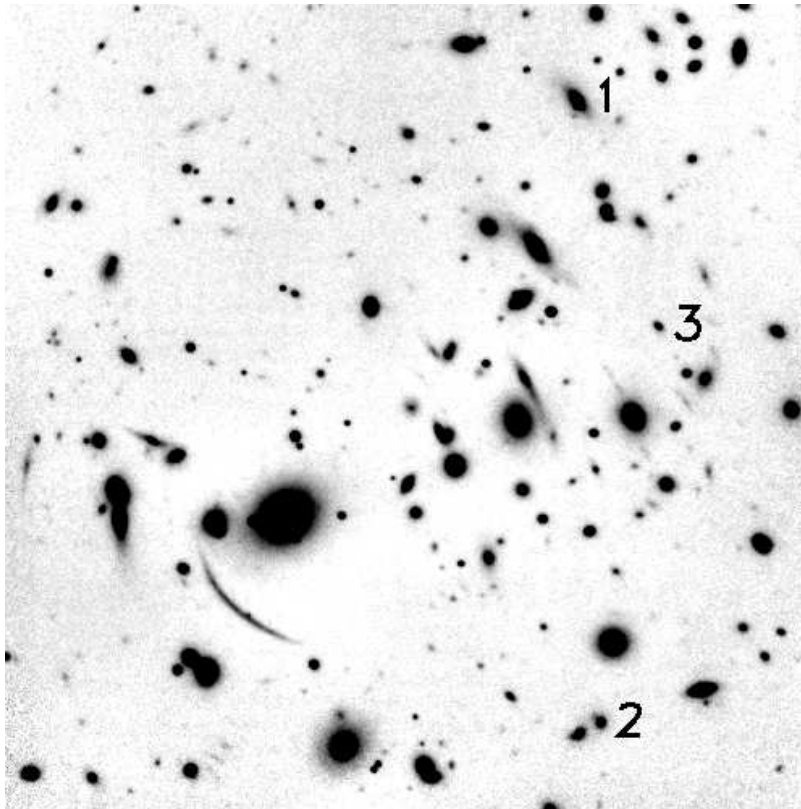


FIG. 1.— K' image of the A2390 field with the three X-ray sources marked. In each case the galaxy corresponding to the X-ray source lies immediately to the left of the number. The numbering corresponds to the listings in Table 1, which is ordered by NIR magnitude. Coordinates (J2000) are: (Source 1) RA: 21:53:34.03 Dec: 17:42:42.5, (Source 2) RA: 21:53:33.75 Dec: 17:41:16.8, (Source 3) RA: 21:53:33.23 Dec: 17:42:11.3.

population.

The coordinates and properties of the three X-ray sources behind A2390 are summarized in Table 1 and in the caption of Fig. 1. Magnitudes are measured in $2''$ diameter apertures. We have applied a small differential correction relative to the K' magnitudes to allow for differences in the image quality between the bands: $-0.02(H)$, $-0.04(J)$, $0.03(I)$, $-0.08(R)$, $-0.18(V)$, and $-0.17(B)$. In the fitting procedures we have also allowed for a 0.2 magnitude systematic uncertainty over the statistical errors in Table 1. Where total magnitudes are required, the offsets to the isophotal magnitudes of the final column of the table should be used. The X-ray coordinates have been offset to match the optical data. The Source 2 X-ray position has also been updated from that given in Fabian et al. (2000) and now has a clear optical counterpart.

2. OBSERVATIONS

2.1. Near-infrared Imaging

We used the new Cooled Infrared Spectrograph and Camera for OHS (CISCO, Motohara et al. 1998) on the Subaru 8.3 m telescope UT 2000 June 18–19, July 15–16, September 10–12, and November 7 to obtain extremely deep J , H , and K' images of the clusters A2390 and A370. The detector used was a 1024×1024 HgCdTe HAWAII array with a pixel scale of $0.111''$ for the June, July, and November runs and a pixel scale of $0.105''$ for the September run. This provides a field-of-view $\sim 2' \times 2'$. The data were taken in unguided mode and therefore relied on the superb telescope tracking to maintain image quality. To minimize the image degradation, a number of sub-

exposures were taken at each position in an eight-point pentagon pattern ($5''$ step size). The weather conditions were photometric, and the seeing was typically $0.3'' - 0.5''$ during the first three observing runs, which was also the resolution for nearly all the final reduced images. Conditions were clear but with variable seeing during the November run, with characteristic image FWHM of $\sim 0.8''$ for the A370 H image taken on this night. The data were processed using median sky flats generated from the dithered images. The data were calibrated from observations of the UKIRT faint standards (Casali & Hawarden 1992) FS27, FS29, FS6, and FS10. The total exposure times for A2390 were 5520 s (J), 7290 s (H), and 15360 s (K'), and those for A370 were 13280 s (J), 7680 s (H), and 15360 s (K'). The K' image of A2390 is shown in Fig. 1 with the three X-ray sources marked.

2.2. Optical Imaging

Deep multicolor images of A370 were obtained using LRIS on the Keck 10 m telescopes on UT 1999 August 11, September 9–10, and 2000 August 25. The data were taken as a sequence of dithered exposures with net integration times of 4200 s in V , 4800 s in R , and 2700 s in I . The data were processed using median sky flats generated from the exposures. Conditions were photometric during the observations. The V , R , and I data were calibrated using the photometric and spectrophotometric standard HZ4 (Turnshek et al. 1990; Oke 1990) and faint Landolt standard stars in the SA 95-42 field (Landolt 1992). Deep B (3780 s) and R (2940s) images of A370 were obtained with ESI on Keck II on UT 2000 September 29–30.

For A2390, B (3600 s), R (1800 s), and I (1080 s) images were obtained using ESI on the Keck II telescope on UT 2000 November 29–30. The V (4200 s) image was obtained on UT 2000 September 29. The data were calibrated with faint Landolt standards in the fields of SA 113-337 and SA 95-42 (Landolt 1992).

2.3. Near-infrared Spectroscopy

We used CISCO on UT 2000 November 7 with the zJ grating to obtain NIR spectra of two of the A2390 sources (Sources 1 and 2). The zJ grating setup provides wavelength coverage over the range $\lambda\lambda 8450\text{--}14100\text{ \AA}$, with a steep decline in sensitivity below $\sim 8750\text{ \AA}$. We used a $1''$ wide slit for the observations, which provides a resolution of about $R=280$ over this wavelength range, as measured from the FWHM of the neon calibration lines and spectral emission features in the targets. We took 400 s exposures using a 2-point dither with $5''$ separation along the slit at eight positions for Source 1, for a total of 3200 s, and at ten positions for Source 2, for a total of 4000 s. A second order polynomial fit for the wavelength was obtained from night sky lines and Paschen series lines in A type spectral template stars, and the zero-point was adjusted to the position of OH sky lines in the target observations.

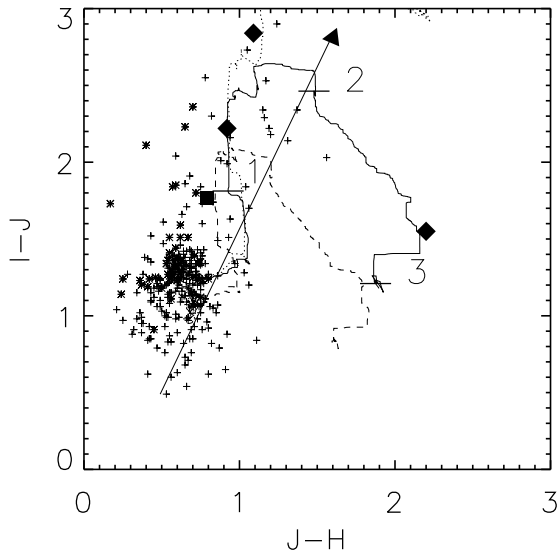


FIG. 2.— The $I - J$ versus $J - H$ colors for the sources in the A2390 and A370 CISCO fields are shown by crosses, with compact sources shown as stars. The four X-ray sources lying behind the clusters and within the NIR area are indicated by filled symbols, with the solid box showing the A370 source and the solid diamonds the A2390 sources. The elongated arrow shows the locus of reddening stretching from an unreddened flat spectrum source to one with $A_V = 10$ magnitudes of reddening. The solid curve shows the colors of an Sa galaxy with redshift in the absence of any evolution, using the local ($z = 0$) SED from the Bruzual & Charlot evolutionary code (GISSEL98, Bruzual & Charlot 1993). The colors at redshifts $z = 1, 2,$ and 3 are marked with ticks and labelled. The dotted line shows the same colors for an elliptical galaxy (upper curve) and the dashed line for an Sb galaxy (lower curve).

3. RESULTS AND DISCUSSION

3.1. Colors and SEDs

Figure 2 shows the $I - J$ versus $J - H$ colors of sources detected in the A2390 and A370 CISCO fields. The four X-ray sources are indicated by filled symbols. Only one

of the A370 sources was covered by the infrared images, and it is shown by the solid box. The three A2390 sources are shown as solid diamonds. Point sources are shown as stars. All of the optical counterparts to the X-ray sources are extended. Source 3 lies in an extremely unusual portion of the color-color plane. It has a very large break between the J and H bands and a much flatter $I - J$ color than the trend for the other galaxies. This portion of the plane cannot be reached by reddening any normal galaxy or quasar spectrum. We illustrate this in the figure where we show the locus of a flat spectrum source with reddening as an arrow. The colors are, however, consistent with a present-day Sa located at a redshift near 3. The remaining three X-ray sources, including the A370 galaxy known to be at $z = 1.060$, are consistent with being similar galaxies in the $z = 1 - 2$ range.

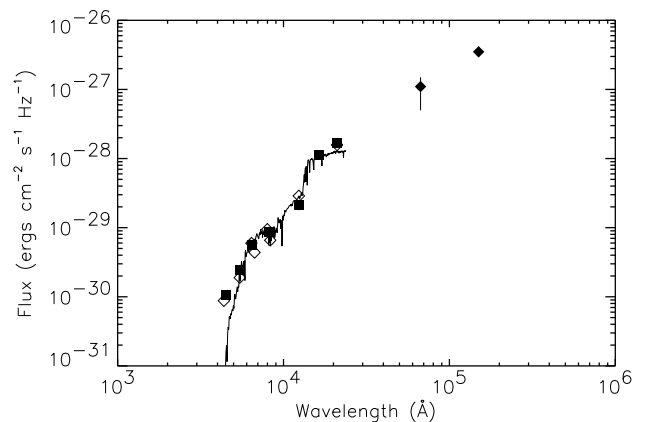


FIG. 3.— Observed SED for Source 3. The $B, V, R, I, J, H,$ and K' fluxes from the present data are shown as solid squares: the HST and ground-based data from Lémonon et al. (1998) are shown as open diamonds together with their ISOCAM points (solid diamonds). Error bars (where shown) are 1σ . The best-fit model from *hyperz* is overlaid.

The red optical to NIR colors of these galaxies therefore appear to be a consequence of the SEDs rather than of dust reddening. The morphologies also show no color differentiation. This would not be expected if a reddened nucleus were beginning to appear at the longer wavelengths. Photometric redshift fitting should be quite robust for this type of source.

3.2. Photometric Redshifts

We used the *hyperz* photometric fitting routine of Bolzonella, Pelló, & Miralles (2001) and our observed $B, V, R, I, J, H,$ and K' magnitudes to estimate redshifts for the X-ray sources. The *hyperz* program compares the observed SED of the galaxy to a set of template spectra generated with the Bruzual & Charlot evolutionary code (GISSEL98, Bruzual & Charlot 1993). We used the eight synthetic star formation histories constructed to match the observed properties of local field galaxies from type E to Im. We assumed no reddening.

Figure 3 shows the observed SED (solid squares) of Source 3 with its deep break between the J and H bands. The best-fit solution from *hyperz* is overlaid on the observed SED. The photometric redshifts for the three X-ray sources behind A2390 are $z_{phot} = 1.4(1.3 - 1.6)$ (Source 1), $z_{phot} = 1.5(1.3 - 1.7)$ (Source 2), and $z_{phot} = 2.6(2.4 - 2.7)$

(Source 3), where the bracketed numbers are the 90% confidence ranges. All of the SEDs are adequately fit by single burst models. The youngest source (age 5×10^8 yr) is also the highest redshift source (Source 3). While the photometric redshift estimates are not sensitive to the details of the models, the age estimate is affected by the choice of cosmology and the choice of models. For example, a lower metallicity would require a larger age. The source behind A370 is found to have $z_{phot} = 1.0(0.8 - 1.2)$, consistent with its spectroscopic redshift $z_{spec} = 1.060$. The inclusion of reddening does not change the redshift estimates.

We note that Lémonon et al. (1998) and Wilman, Fabian & Gandhi (2000) put Source 3 at $z_{phot} \simeq 0.5-0.6$. The addition of the *H* band data breaks the degeneracy in the redshift information and places the source at a much higher redshift in order to reproduce the strong *J-H* break.

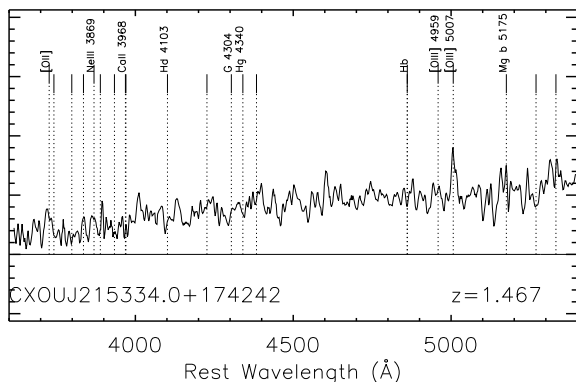


FIG. 4.— CISCO NIR spectrum of Source 1 at $z_{spec} = 1.467$. The [OII] 3727 and [OIII] 5007 lines are clearly visible in the spectrum, along with the Ca H and K absorption lines.

3.3. Spectroscopic Redshifts

Subsequent to estimating the photometric redshifts we obtained spectra of Sources 1 and 2 with CISCO. Source 1 (Fig. 4) has an unambiguous redshift of 1.467, based on the detection of [OII] 3727 and [OIII] 5007. The weaker [OIII] 4959 feature was too faint to be detected. The [OII] 3727 line was confirmed with a one hour spectrum ($\lambda\lambda 6000 - 10000$ Å, $1.4''$ wide slit, ~ 12 Å resolution) taken with LRIS on Keck I on UT 4 October 2000. This higher resolution spectrum yielded a redshift of 1.466. The apparent weakness of the emission lines in the spectrum is a consequence of the low resolution of the infrared spectroscopic observations, and the equivalent widths of the lines are quite representative of other field galaxies at these redshifts.

Source 2 has only a single line which, if interpreted as [OIII] 5007, would also place this source at 1.467, consistent with the photometric estimate. [OII] 3727 is not clearly present, however, so it is also possible that this line could be [OIII] 5007, placing the galaxy at $z_{spec} = 2.317$. No LRIS spectrum is presently available for this source.

A one hour LRIS spectrum was also obtained for Source 3 covering the 6000 to 10000 Å region, but, as is reason-

able given the faintness of the source, no features could be clearly seen.

3.4. Longer wavelengths

Based on ISOCAM data (Lémonon et al. 1998, Altieri et al. 1999) all three of the galaxies have significant excess flux in the mid-infrared wavelengths over and above the galaxy light (see Fig. 3), while none have strong 850 micron detections (Fabian et al. 2000; Barger & Kneib 2001). This longer wavelength excess in the infrared and the absence of strong submillimeter light is best interpreted with a model of hot dust surrounding the central AGN, as discussed in Wilman, Fabian & Gandhi (2000). We postpone a more detailed discussion to a subsequent paper.

4. CONCLUSIONS

The present observations, while based on a small sample, appear to confirm that many of the optically faint *Chandra* sources lie in luminous high redshift galaxies which are relatively evolved. All three X-ray sources behind A2390 lie in red galaxies with redshifts between $z = 1.4$ and $z = 3$. The observed absolute *K'* magnitudes are $[-27.1, -26.5, -26.7]$ for sources [1,2,3], where Source 1 is placed at its spectroscopic redshift and Sources 2 and 3 at their photometric redshifts of $z_{phot} = 1.5$ and $z_{phot} = 2.5$. When the cluster magnification of [2.1,2.8,7.8] and the aperture to isophotal correction is accounted for, these become $[-27.2, -25.8, -24.8]$, where all absolute magnitudes are calculated for $H_0=65$ and an $\Omega = \frac{1}{3}$, $\Lambda = \frac{2}{3}$ Universe. Thus, the galaxies are comparable to or slightly more luminous than the local L_* . When corrected for magnification, the 2–7 keV X-ray luminosities lie in the 10^{44} to 10^{45} erg s^{-1} range. All of the sources have significant excess light in the mid-infrared, presumably as a result of reprocessing of the AGN light by hot dust (Wilman, Fabian & Gandhi 2000).

The very large magnification of the evolved high redshift Source 3 is the key to its identification. There may be numerous objects of this type in field samples which are simply too faint to pick out using NIR color selection. The combination of very deep hard X-ray and optical data will allow us to select such sources for intensive study. For the highest redshift source, the demagnified X-ray flux would be 3×10^{-15} erg $cm^{-2} s^{-1}$ and the *I* magnitude would be 26. It is at these levels that we may find further examples in the field samples.

AJB acknowledges support from NASA through Hubble Fellowship grant HF-01117.01-A awarded by the Space Telescope Science Institute, which is operated by the Association of Universities for Research in Astronomy, Inc., for NASA under contract NAS 5-26555. AJB, LLC, and EMH acknowledge support from NSF through grants AST-0084847, AST-0084816 and AST-0071208, and CSC and ACF thank the Royal Society for support. We would like to thank Rolf Kudritzki and Toni Songaila for critically reading the first draft of this paper.

REFERENCES

- Altieri, B., et al. 1999, *A&A*, 343, L65
 Barger, A.J., Cowie, L.L., Smail, I., Ivison, R.J., Blain, A.W., & Kneib, J.-P. 1999, *AJ*, 117, 2656
 Barger, A.J., Cowie, L.L., Mushotzky, R.M., Richards, E.A. 2001, *AJ*, in press (astro-ph/0007175)
 Barger, A.J., Kneib, J.-P. 2001, in preparation
 Bautz, M.W., Malm, M.R., Baganoff, F.K., Ricker, G.R., Canizares, C.R., Brandt, W.N., Hornschemeier, A.E., Garmire, G.P. 2000, *ApJ*, 543, L119
 Bolzonella, M., Pelló, R., Miralles, J.-M. 2000, *A&A*, in press (astro-ph/0003380)
 Bruzual, G., Charlot, S. 1993, *ApJ*, 405, 538
 Casali, M., Hawarden, T. 1992, *JCMT-UKIRT Newsletter*, 4, 33
 Crawford, C.S., Fabian, A.C., Gandhi, P., Wilman, R.J., Johnstone, R.M. 2001, *MNRAS*, submitted (astro-ph/0005242)
 Fabian, A.C., et al. 2000, *MNRAS*, 315, L8
 Giacconi, R., et al. 2001, *ApJ*, in press (astro-ph/0007240)
 Hornschemeier, A.E., et al. 2001, *ApJ*, in press (astro-ph/0101494)
 Ivison, R.J., et al. 1998, *MNRAS*, 298, 583
 Landolt, A.U. 1992, *AJ*, 104, 340
 Lémonon, L., Pierre, M., Cesarsky, C.J., Elbaz, D., Pelló, R., Soucail, G., Vigroux, L. 1998, *A&A*, 334, L21
 Motohara, K., et al. 1998, *Proc. SPIE* 3354, 659
 Mushotzky, R.F., Cowie, L.L., Barger, A.J., Arnaud, K.A. 2000, *Nature*, 404, 459
 Oke, J.B., 1990, *AJ*, 99, 1621
 Soucail, G., Kneib, J.-P., Jaunsen, A.O., Hjorth, J., Hattori, M., & Yamada, T. 1990, *A&A*, 343, L70
 Smail, I., Ivison, R.J., Blain, A.W. 1997, 490, L5
 Turnshek, D.A., Bohlin, R.C., Williamson II, R.L., Lupie, O.L., Koornneef, J., & Morgan, D.H. 1990, *AJ*, 99, 1243
 Wilman, R.J., Fabian, A.C., Gandhi, P. 2000, *MNRAS*, 318, L11

TABLE 1
 X-RAY SOURCES BEHIND A2390 CLUSTER

CXSOUJ Source Name	Soft/Hard X-ray Fluxes ^a	<i>B</i> (mag)	<i>V</i> (mag)	<i>R</i> (mag)	<i>I</i> (mag)	<i>J</i> (mag)	<i>H</i> (mag)	<i>K'</i> (mag)	<i>K'iso</i> ^b (mag)
215334.0+174242	9.9/90	26.11 ± 0.40	25.39 ± 0.22	23.93 ± 0.08	22.17 ± 0.06	19.33 ± 0.01	18.24 ± 0.00	17.41 ± 0.01	16.5
215333.8+174116	3.7/ < 17	24.32 ± 0.09	23.64 ± 0.04	22.76 ± 0.03	22.09 ± 0.06	19.87 ± 0.02	18.95 ± 0.01	18.15 ± 0.01	17.7
215333.2+174211	5.9/23	26.27 ± 0.45	25.25 ± 0.16	24.23 ± 0.11	23.67 ± 0.20	22.12 ± 0.14	19.92 ± 0.02	19.05 ± 0.03	18.8

^a0.5-2.0 keV/2-7 keV X-ray fluxes given in units of 10^{-15} erg cm⁻² s⁻¹

^bIsophotal magnitude to 2% of peak surface brightness